Pulmonary lobar segmentation from computed tomography scans based on statistical finite element analysis of lobe

Zhang, Y.[1], Osanlouy, M.[1], Clark, A.R.[1], Hoffman, E.A.[2], Tawhai, M.H[1]

[1]Auckland Bioengineering Institute, University of Auckland, Auckland, NZ, [2]Department of Radiology and Biomedical Engineering, University of Iowa Carver College of Medicine, Iowa City, IA, US.

Abstract

Automatic identification of pulmonary lobes from imaging is important in lung disease assessment and treatment planning. However, the pulmonary lobar fissure can be difficult to detect automatically, as it is thin, usually fuzzy appearance and incomplete, and can be obscured by or confused with features of disease. In this study, we aim to overcome difficulties in identifying pulmonary fissures by using a statistical finite element analysis of lobe (SFeaL) to guide lobar segmentation. By deforming an average lobar model onto an individual's lung shape, we predict fissure locations approximately, to refine our search region for lobar structures. Then, we use an eigenvalue of Hessian matrix analysis and a connected component eigenvector based analysis to determine a set of fissure-like candidate points. A smooth multi-level B-spline curve is fitted to the most fissure-like points (those with high fissure probability) and the fitted fissure plane is extrapolated to the lung boundaries. The method was tested on 20 inspiratory and expiratory CT scans in healthy young subjects and older subjects with idiopathic pulmonary fibrosis. A quantitative evaluation showed that the mean difference of left oblique, right horizontal and right oblique fissure to the reference was 2.06mm, 4.06mm and 2.85mm for healthy cases and 3.41mm, 5.79mm and 5.01mm for pathological cases.

1 Introduction

Human lungs are divided into five lobes which form distinct anatomical regions separated by fissures. Identification of these lobes in imaging is of great importance for assessment of lung disease severity and treatment planning. The lobes act independently of each other with respect to respiratory function, thus many pulmonary diseases act as a lobar level [1]. For example, emphysema, postprimary tuberculosis and silicosis usually affect the upper lobes, while idiopathic pulmonary fibrosis is commonly present in the lower lobes. For clinical applications, identification of the pulmonary fissures can be an important step in the image-based study of lung function and disease, thus the distribution of pulmonary disease are beneficial for doctors to recognize pathogenesis, guide therapy and have further value in surgical planning [2]. Meanwhile, segmentation of pulmonary lobes can also drive intra-patient registration, since lobes are important landmarks and allow us to localize disease progression. However, the lobes are difficult to segment automatically as they can appear as faint or fuzzy lines in imaging, fissures can be incomplete (even in healthy patients), and there is anatomical variation in lobe shape and size between individuals. This anatomical variation is usually associated with age, sex, height and body mass index (BMI)

批注 [Office1]: These two sentences effectively say the same thing and don't give a strong motivation for lobar segmentation. Papers I have found give lots of reasons which don't come across here (definitely needs more references and examples):

- Relative functional independence of lobes – because they are independent they logical way to divide the lung when assessing disease distribution, and are likely candidates for surgical removal
- Disease classification: Some diseases are almost exclusively localized to certain lobes of the lung, particularly in early stages, and being able to identify lobar distributions of abnormalities in imaging helps to diagnose pathology and understand the impact of certain pathologies on whole lung function (e.g. ventilation perfusion matching.
- Intra-patient registration: Lobes are important landmarks when registering within patient imaging (eg changes in lung tissue over time) and allow us to localize disease progression
- Operative planning: e.g. emphysema patients benefit most from surgery if disease is in apical lobes. Identifying lobes allows us to determine how localized is disease and what are the possible implications of removing portions of the lung.

[3] [4].

In a broad sense, existing algorithms that aim to automatically segment pulmonary lobes consist of two steps: lung segmentation and fissure detection. Lung segmentation methods are well-established and results are typically reliable [5] [6] [7]. In contrast, automated fissure detection is challenging. Some proposed fissure detection methods make use of either local or global knowledge of lung anatomy, such as airway and vessel trees, to identify fissures [1] [8] [9]. For example, there are not typically any large vessels in the vicinity of lobar fissures, so fissures should be located in the gaps between airway and vessel trees. These methods can be time consuming as airways and blood vessels must be identified as an intermediate step. A second class of fissure detection algorithm makes use of gray-level information and shape information to detect the fissures [2] [3] [10]. Generally, lobar fissures can be regarded as bright planes crossing the pulmonary volume because of the higher density value of fissures comparing to the surrounding tissues. Based on this information, several published methods use local filtering algorithm to detect the voxels which lie on these planes, so that these detected voxel points can construct a continuous fissure surface. These algorithms often face problems when lobe fissures are blurry or incomplete.

In this paper, we propose a statistical finite element analysis of lobe (SFeaL) model guided method to segment pulmonary lobes from CT images. Our new procedure does not depend on prior segmentation of anatomical structures (airway lobar classification) and has promising potential as a clinically useful automatic lobe segmentation procedure. A user-interactive interface is also developed for user to control and visualize the whole segmentation process and, if necessary, do some manual correction on the segmentation results.

2 Methods

We follow a three-step approach for lobe segmentation (Fig 1): in the first step, a threshold-based lung segmentation method defines the lung boundary. In the second step, a statistical shape model (SSM) is deformed provide a 'search region' for fissure locations. In the third step, fissures are located using a Hessian matrix protocol combined with connected component filters and surface fitting algorithm.

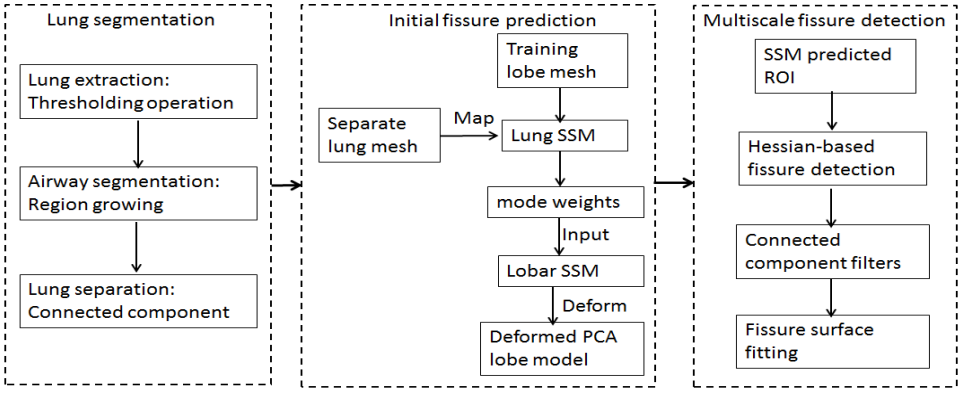

Fig. 1. Flow diagram of the lobar segmentation process.

2.1 Lung segmentation

Here we use commonly used thresholding method to segment lungs [6]. The method uses a thresholding operation (-775 Hounsfield Units) and connected component identification to find an initial approximation to the lung regions and trachea location. Using the most apical point of trachea as a start point, a region growing technique is applied to detect the airway trees. Then, left and right lungs are separated as the two largest connected components remaining after removing the trachea and main left and right bronchi.

2.2 Statistical finite element analysis of lobe model

A Statistical Finite element analysis of Lobe (SFeaL) which is based on an active shape model (ASM) [11] of the lung is constructed and deformed onto the individual's images to predict an initial fissure to guide fissure detection. The SFeaL model was constructed using a training set consisting of imaging of the lung …. 30 healthy non-smokers (15 males and 15 females) subjects were selected from the Human Lung Atlas (HLA) database as the training data. The open-source visualization software CMGUI (https://www.cmiss.org/cmgui) was employed to manually click all three fissure points between adjacent lobes by an expert user to provide a gold-standard fissure location for each subject in the training set.

A finite element volume mesh is used to describe the shape of the lung and its fissures both in terms of the ASM and also to define initial fissure location in the segmentation algorithm. A high order (bi-cubic Hermite) finite element mesh template was fitted to lung surface data obtained from the lung segmentation (Section 2.1). The template mesh for the left lung mesh has 35 nodes and 44 elements, while the right lung mesh has 50 nodes and 62 elements. Each node has 12 degrees of freedom (DoF) which store the global coordinates and first and second nodal derivatives. These nodes were selected to represent critical anatomical locations, such as the apex, the base vertex , the shape corner and the center point of the middle line of fissure. A least squares fit of the mesh to the lung surface data was conducted using CMISS (https://www.cmiss.org), a finite element modeling environment. The average root mean square (RMS) error of this fitting method was 0.52mm for the 30 training subjects (Fig 2(a)).

To construct the SSM, each node in the finite element mesh was used as a pseudo-landmark and a principal component analysis (PCA) conducted on the training set. To remove the orientation and scaling differences between shapes, a general procrustes alignment (GPA) method was used to minimize the distance between subjects through calculating the optimal rotation matrix and translation (Fig 2(b)) [12]. The volumes of all the subjects were normalized to 1L during the processing. The procrusted aligned meshes is represented by

$$\mathrm{B} = [\overline{x_1}\ \overline{y_1}\ \overline{z_1}\ \overline{x_2}\ \overline{y_2}\ \overline{z_2} \cdots \overline{x_p}\ \overline{y_p}\ \overline{z_p}],$$

where p is the total node number of all the subjects (2550 nodes for our study, 30 subjects in total), and the over-line represents GPA to the mean. The matrix B was then decomposed into modes of variation by a PCA [13]. Each mode symbolizes one type of lobe shape variation. PCA is a statistical procedure using an orthogonal transformation to help us find the principle components, which here are the modes with the most lobe shape variation through analyzing the eigenvectors and eigenvalues of the covariance matrix of the data matrix B. The results of principle components of variation showed that the first seven principal components account for over 90%

批注 [Office2]: Here you need to describe the data that went into building the statistical shape model, including how fissures were segmented for these subjets

批注 [Office3]: Do any nodes have defined anatomical locations, what is done to ensure they can be used as pseudo landmarks.

批注 [Office4]: If you are short of space some of this info could be removed.

of the total variation. The PCA provides a definition of a statistically averaged lobar shape.

2.3 Initial prediction of lobar location in an individual

To predict the fissure locations in volumetric CT imaging from a subject not part of the training cohort a finite element mesh of the lung surface (without fissure information) is generated for this subject. This lung surface mesh is projected on to the PCA-trained average lung statistical mesh (no fissure surfaces). The principal component weight values were calculated from the projection and these weights were then used on the deformation of PCA-trained average lobar statistical mesh (with fissure surfaces) to derive an initial estimation of fissure locations (Fig 2(c) (d)). This initial SFeaL based prediction of lobar fissures provides a reduced search area for subsequent image analysis and ensures definition of complete lobar structures even if a fissure is incomplete or difficult to detect in a small region of the image.

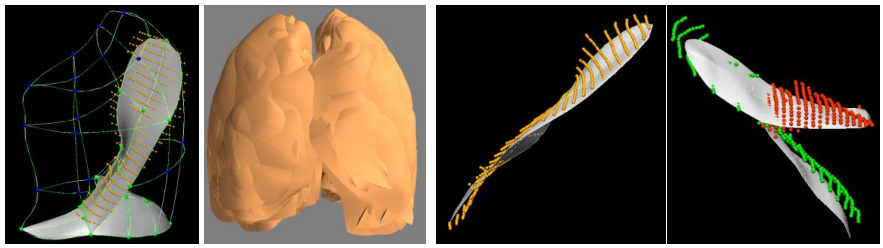

(a) (b) (c) (d)

Fig. 2. SFeaL based initial fissure prediction results. (a) Lung surface fitting and fissure digitizing manually. (b) Procrustes aligned meshes of 30 subjects. (c) (d) Fissure prediction compared to manual tracing points. White mesh is the predicted fissure surfaces.

2.4 Multiscale Hessian-based fissure detection

The location of SFeaL predicted fissure planes (Fig 3d) are used to guide a Hessian based fissure detection in an individual. Gaussian filters with a range of kernel sizes (0.5mm, 1.0mm, 1.5mm, 2.0mm, 2.5mm) were applied to the image set. The responses at each kernel are combined to get a maximum response for each voxel of the image. This multiscale operation guarantees fissures of variable size can be captured by Hessian operations. At each image voxel, the Hessian matrix was constructed as a symmetric matrix. For a fissure structure, which presents as a light plane on a dark background, two large positive second derivatives across the plane and a small second derivative (of either sign) along the plane are expected. This is reflected in the Hessian matrix as two small eigenvalues corresponding to the eigenvectors along the fissure planes and one large eigenvalue perpendicular to the plane. Thus with the relationship of eigenvalues λ_1, λ_2, λ_3 is defined as $|\lambda_1| \leq |\lambda_2| \leq |\lambda_3|$. λ_3 is expected to much larger than λ_1 and λ_2 at the fissure. From these characteristics, we can get a fissure probability of each voxel derived as follows:

$$S = \tau S_{plane} S_{wall}.$$

The parameter τ surpresses points whose largest eigenvalue $\lambda_3$is positive, since fissures are locally bright , and is defined as

批注 **[Office5]:** Can you specify how many and where they sit in the range if this is always the same

$$\tau = \begin{cases} 1, \lambda_3 < 0 \\ 0, \lambda_3 \geq 0 \end{cases}.$$

S_{plane} detects plane or curve-like structures by searching for locations where $|\lambda_3|$ and $|\lambda_2|$ are significantly different:

$$S_{plane} = \exp(-\frac{{S_{plane}}^2}{2p^2}),\ R_{plane} = \frac{|\lambda_2|}{|\lambda_3|}$$

S_{wall} suppresses signals of noise and blob-like structures:

$$S_{wall} = \exp(-\frac{{R_{noise}}^2}{2w^2}),\ R_{noise} = \sqrt{\lambda_1^2 + \lambda_2^2 + \lambda_3^2}$$

S then gives a high response to local sheet-like structures such as fissures and suppresses other pulmonary structures. An example of a fissure enhancement filter applied in an individual is shown in Fig 3(a).

Blood vessels, which appear as similar structures locally to fissures are removed from the fissure enhanced result using previous described methods, which removes tube-like structures with $|\lambda_1| \approx 0, |\lambda_1| \ll |\lambda_2|,\ |\lambda_2| \approx |\lambda_3|$ (Fig 3(b)) [14].

The fissure location predicted by the SFeaL allows definition of a search region for the fissure (Fig. 3(c)). Candidate points are selected within a certain distance of the initial fissure approximation. The search distance was set to 20 voxels for left and right oblique fissure and 15 voxels for right horizontal fissure. A 2D 4-neighborhood connected component filter and a 3D 6-neighborhood vector-based connected component filter are employed successively to eliminate noise arising from small plane-like structures in this search region (Fig 3(d)). The vector-based connected component filter uses the inner product of the normalized largest eigenvector of the Hessian matrix in adjacent voxels. These largest eigenvectors are perpendicular to the fissure plane, and their inner product provides a criterion for component connection. As fissure curvature of a fissure is locally low, adjacent fissure voxels should have similar largest eigenvectors and thus large inner product values.

批注 **[Office6]:** Define the distance

The detected points are then divided into a set of small subsections corresponding to different x, y intervals. For each subsection, the point of the highest fissure probability (the highest S value) is selected as the finial candidate fissure point (Fig 3(e)). Then a continuous smooth fissure surface is generated using a B-spline method with a thin-plane spline and extrapolated to the lung boundaries, see Fig 3(f).

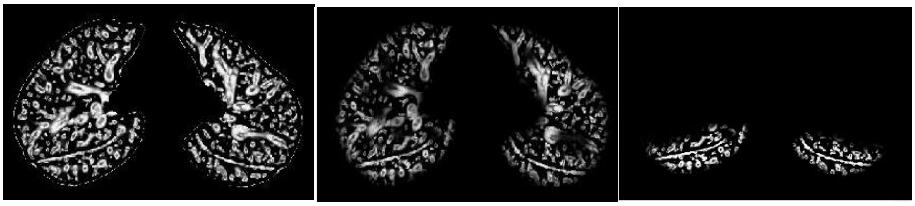

(a) (b) (c)

(d) (e) (f)

Fig. 3. Hessian-based multiscale fissure detection results. (a) Hessian-based fissure enhancement. (b) Remove vessel voxels. (c) ROI of fissure locations based on SSM projection. (d) 2D and 3D eigenvector based connected component filter. (e) Fissure candidate points. (f) B-spline curve fissure surface fitting.

3 Experiment

3.1 Data

We tested our automatic lobar segmentation method on two datasets : 1) CT images of young normal volunteers taken at different lung volumes and with different thickness 2) Clinical CT images of old patients diagnosed with idiopathic pulmonary fibrosis (IPF) disease. Normal subjects were selected from Human Lung Atlas (HLA) dataset which is approved by the University of Iowa Institutional Review Board and Radiation Safety Committees. The selected subjects are consists of 5 functional residual capacity (FRC) cases and 5 total lung capacity (TLC) cases. Slice thickness was 0.5-0.7mm. These diseased subjects are acquired from Auckland District Health Board (ADHB) under the supervision of Dr. Wilsher, following ethics committee approval for this study. Slice thickness was 1.25-3mm.

批注 **[Office7]:** For Merryn to change but needs to be reworded

3.2 Result

To assess the accuracy of the automatic lobar segmentation method in the normal and disease subjects, we compared the automatic segmentation results to gold-standard manual segmentations. Segmentation accuracy was quantitatively evaluated by computing the mean difference and percentage of fissure points <3mm between gold-standard and automatic segmentations (Fig 4). The 3mm criterion approximates the thickness of clinical CT images that surgeons and radiologists read in clinical settings [15].

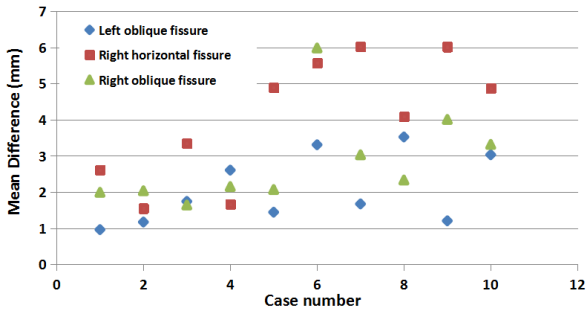

(a)

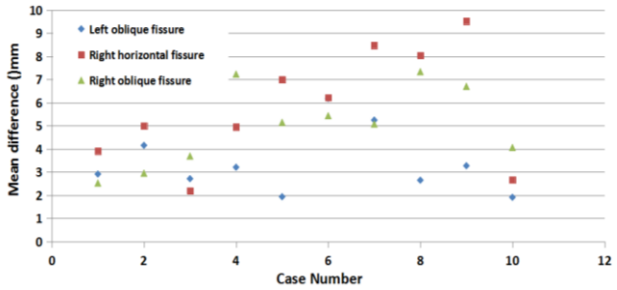

(b)

Fig. 4. Quantitative evaluation results of the segmentation accuracy. (a) Mean difference of normal young subjects. (b) Mean difference of IPF old subjects.

For normal subjects, the average mean difference are 2.06mm, 4.06mm, 2.85mm, and the average accuracy are 78.39%, 61.62%, 72% for left oblique, right horizontal and right oblique fissure respectively. For IPF abnormal subjects, the average mean difference are 3.41mm, 5.79mm, 5.01mm, and the average percentile accuracy are 65.86%, 55.94%, 60.06% for left oblique, right horizontal and right oblique fissure respectively.

4 Conclusions and Discussions

In this paper, we present a pulmonary lobar segmentation method. The result shows that our segmentation method can perform well on CT images of normal subjects and get a relative accurate result for most of the IPF abnormal subjects. Due to the lower resolution and pathologic abnormalities, IPF subjects got a worse accuracy. In addition, the segmentation method performs well on left oblique fissure than right oblique fissure and right horizontal fissure, because left lung has simpler anatomic structure with only one fissure, in contrast, misdetection happens more often in the area of right lung where the two fissures are closed. See Fig 5, which shows the accuracy distribution of the three fissures with different colors. It can also be seen that the method causes higher error in the lung boundary area, since the fissures here are commonly incomplete, thus few fissure candidate points can be detected accurately.

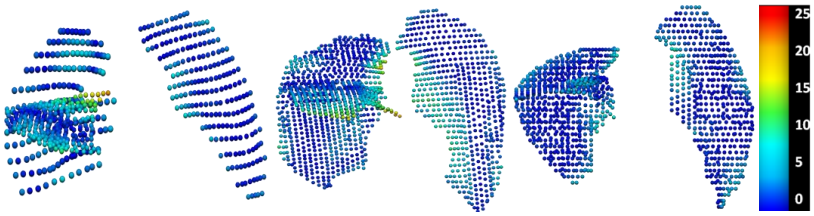

Fig. 5. Accuracy distribution results of some example subjects.

For a successful lobar segmentation，a series of parameter values need to be defined. However, one fixed value of parameter is usually not suitable for all the subjects due to a wide variation of lung tissue and fissure appearances across the population. Therefore, a fast and convenient interactive way to control the segmentation procedure may be necessary on a case by case basis.

批注 [Office8]: This section needs work.
1. What you have presented
2. Accuracy of mthod and comment on reduced accuracy in IPF, note that you can actually segment a fissure in IPF subject which many studies would not
3. Comparison to existing methods (why is it worth using yours)
4. Maybe at this point its appropriate to comment on gui in ptk but only if it is actually being added to the PTK repository for iothers to use
5. Touch briefly on study limitations.

批注 [Office9]: Please define specifically which parameter values

We developed an improved user-friendly interactive interface to control some crucial parameters (including search region distance and connected component analysis size of three fissures) as input. In addition, current published studies show that it seems impossible to ensure one fully automatic lobar segmentation method perform perfectly on all kinds of subjects, especially for some diseased abnormal cases. Therefore, we developed a correction tool on the user interface to improve the result manually.

Compared to the current published anatomical structure based method, our SFeaL based method can predict an initial fissure location without an accurate preliminary analysis of other anatomical tissues. For example, traditional anatomical knowledge based method such as watershed-based lobar segmentation need to label airway trees as five main branches corresponding to five lobes to get an initial fissure approximation. However, due to the disordered distribution of abnormal tissues, it is usually difficult for diseased lungs such as IPF subjects to get a reliable airway and vessel trees segmentation result. After applying the interactive watershed transform method [6] on our IPF subjects, we fail to get initial guessing for nearly half of the subjects, in contrast, our SFeaL method can at least get a reliable segment even though some manual parameter controls and corrections are still necessary.

In the future work, a SFeaL model dataset should be developed. The dataset could contain different kinds of statistical model for different ages, sexes, lung volume or diseases, since it can help us prediction a more accurate region of interest (ROI) for a future fissure detection. Meanwhile, the method need to be assessed on more diseased subjects and be improved combined with different disease characteristics. A user-friendly interaction and more time-saving programming is also a key point in the future study.

Reference

1. Ukil S., Reinhardt J.M.: Anatomy-guided lung lobe segmentation in x-ray CT images. IEEE Transaction Medical Imaging 28(2), 202-214 (2009)

2. van Rikxoort E.M., Prokop M., de Hoop B., Vierggever M.A., Pluim J.P.W., van Ginneken B.: Automatic segmentation of pulmonary lobes robust against incomplete fissures. IEEE Transaction Medical Imaging 29(6), 1286-1296 (2010)

3.Ross J.C, San J.E.R., KindImann G., Diaz A., Westin C.F., Silverman E.K.: Automatic lung lobe segmentation using particles, thin plate splines, and maximum a posteriori estimation. Medical Image Computing and Computer-Assisted Intervention. 13(3) 163-171 (2010)

4. Gülsün M., Ariyürek O., Cömert R., Karabulut N.: Variability of the pulmonary oblique fissures presented by high-resolution computed tomography. Surgical and Radiologic Anatomy. 28(3) 293–299 (2006)

5. Hu S.Y., Hoffman E.A.: Automatic lung segmentation for accurate quantitation of volumetric X-Ray CT images. IEEE Transaction Medical Imaging. 20(6) 490-498 (2001)

6. Ukil S., Reinhardt J.M.: Smoothing lung segmentation surfaces in three-dimensional x-ray CT images using anatomic guidance. Academic Radiology. 12(12) 1502-1511 (2005)

7. Sun S., Bauer C., Beichel R.: Automated 3-D segmentation of lungs with lung cancer in CT data using a novel robust active shape model approach. IEEE Transaction Medical Imaging. 31(2) 449-60 (2012)

8. Doel T., Matin T.N., Gleeson F.V., Gavaghan D.J., Grau V.: Pulmonary lobe segmentation from

CT images using fissureness, airways, vessels and multilevel B-splines. 9th IEEE International Symposium on Biomedical Imaging 1491-1494 (2012)
9. Lassen B., van Rikxoort E.M., Schmidt M., Kerkstra S., van Ginneken B., Kuhnigk J.: Automatic segmentation of the pulmonary lobes from chest CT scans based on fissures, vessels, and bronchi. IEEE Transaction Medical Imaging 32(2) 210-22 (2013)
10. Kitasaka T., Nakada Y., Mori K., Suenaga Y., Mori M., Takabatake H., Natori H.: Recognition of lung lobes and its application to the bronchial structure analysis. 18th International Conference on Pattern Recognition (ICPR'06) 288-291 (2006)
11. Cootes T.F., Taylor C.J., Cooper H.D., Graham J.: Active shape models-their training and application. Computer Vision and Image Understanding 61 38-59 (1995)
12. Rohlf F.J.: Shape statistics: Procrustes supermpositions and tangent spaces. Journal of Classification 16 197-223 (1999)
13. Jolliffe I.: Principal Component Analysis. Springer Series in Statistics (2002)
14. Frangi A.F., Niessen W.J., Vincken K.L., Viergever M.A.: Multiscale vessel enhancement filtering. Medical Image Computing and Computer-Assisted Intervention 130-137 (1998)
15. Qiao W.: Segmentation of lung lobes in high-resolution isotropic CT images. IEEE Transactions on Biomedical Engineering 56(5) (2009)